IEEE Access
Multidisciplinary | Rapid Review | Open Access Journal

Received 5 March 2024, accepted 18 March 2024, date of publication 25 March 2024, date of current version 29 March 2024.

Digital Object Identifier 10.1109/ACCESS.2024.3380471

RESEARCH ARTICLE

Estimation of Chromophpric Dissolved Organic Matter Concentration in Erhai Lake Using the Quasi-Analytical Algorithm From Sentinel-3 Satellite Data

ZHENGNAN ZENG[1,2], BO-HUI TANG[1,2,3], (Senior Member, IEEE), DONG WANG[1,2], (Student Member, IEEE), LIANG HUANG[1,2], GUOKUN CHEN[1,2], AND ZHONGXI GE[1,2]

[1]Faculty of Land Resources Engineering, Kunming University of Science and Technology, Kunming 650093, China
[2]Key Laboratory of Plateau Remote Sensing, Department of Education of Yunnan Province, Kunming 650093, China
[3]State Key Laboratory of Resources and Environmental Information System, Institute of Geographic Sciences and Natural Resources Research, Chinese Academy of Sciences, Beijing 100101, China

Corresponding author: Bo-Hui Tang (tangbh@kust.edu.cn)

This work was supported in part by the National Natural Science Foundation of China under Grant 42230109, in part by the Platform Construction Project of High-Level Talent in Kunming University of Science and Technology (KUST) under Grant 41961053, and in part by Yunling Scholar Project of the "Xingdian Talent Support Program" of Yunnan Province.

ABSTRACT Chromophoric dissolved organic matter (CDOM) is a crucial component of aquatic environments. Accurately quantifying the content of CDOM is essential for supporting lake water quality monitoring and management. In this study, we utilized quasi-analytical algorithms (QAA_v6 and QAA_CDOM) to estimate the CDOM concentration in the intricate freshwater environment of Erhai Lake. This was accomplished by utilizing in-situ hyperspectral data and water sample measurements. A quasi-analytical algorithm, named QAA_CDOM_680, was proposed to retrieve CDOM absorption coefficients from Sentinel-3 satellite images by optimizing the reference wavelength based on these two algorithms. The root mean square errors (RMSE) for QAA_V6, QAA_CDOM algorithm, and the new algorithm QAA_CDOM_680 are 0.615, 0.2235, and 0.1935, respectively. The calibration determination coefficients (R^2) of the three algorithms are 0.44, 0.51, and 0.63, respectively. The new algorithm demonstrates a significant improvement in accuracy. The results of two satellite-ground synchronous inversions indicate that the calibration determination coefficients (R^2) of CDOM absorption coefficients in the Erhai Lake research area are 0.42 and 0.48, respectively. This study has successfully completed the dynamic quantification monitoring of CDOM in Erhai Lake, contributing to the preservation of Erhai Lake's water quality.

INDEX TERMS Chromophoric dissolved organic matter (CDOM), quasi-analytical algorithm (QAA), Sentinel-3 OLCI, Erhai lake.

I. INTRODUCTION

Dissolved organic matter (DOM) is an important component of organic carbon in water bodies, always affecting the biological activities and material cycles in the aquatic environment, and the spatial and temporal dynamics of dissolved and suspended organic matter in water reflect the cyclical changes of carbon in water [1]. Among them, the colored component of dissolved organic matter (DOM) is referred to as chromophoric dissolved organic matter (CDOM). CDOM, commonly referred to as yellow matter or soluble organic chromophores [2]. CDOM is mainly composed of humic acid, fulvic acid, etc., and the main sources are soil organic matter, planktonic algae, and aquatic plant degradation [3]. The main source of CDOM in one class of oceanic waters is the auto-degradation of phytoplankton. For nearshore waters,

The associate editor coordinating the review of this manuscript and approving it for publication was Jon Atli Benediktsson.

CDOM is influenced by exogenous inputs; for inland complex waters, it is influenced by both exogenous inputs and phytoplankton degradation [4]. CDOM is a chromogenic component of dissolved organic matter in water, exhibiting strong absorption properties in the ultraviolet and visible spectra, and it plays a vital role in the carbon cycling process within water bodies and measuring the concentration of dissolved organic carbon (DOC) [5]. High concentrations of CDOM in the water column limit biologically harmful UV-B radiation and protect phytoplankton and other light-sensitive organisms in the water column [2]. At the same time, CDOM effectively reduces the penetration of effective photosynthetic radiation in the underwater light field and is an important indicator of primary productivity [6]. Through conducting remote sensing monitoring research on key parameters of the aquatic ecosystem in the Erhai Lake basin, we have achieved a comprehensive understanding of the dynamic changes in the region. This enables us to provide scientifically sound recommendations to local governments, environmental protection agencies, and urban planning departments, thereby promoting the sustainable development of the ecological environment in the area.

Remote sensing platforms are able to generate the spatial distribution of CDOM on a large scale. The spectral characteristics of CDOM are similar to those of non-algal particles (NAP), and the CDOM light absorption properties are not the same as those of phytoplankton [7]. CDOM, chlorophyll, non-algal particles, and suspended particles all contribute to changes in the underwater light field, which subsequently affect the water-leaving radiation detected by satellite sensors. As a result, remote sensing techniques can be utilized to estimate CDOM concentrations over large spatial scales [8]. Currently, some research has been conducted on the inherent optical properties and water color remote sensing inversion models of Erhai Lake, but most of them are based on empirical or semi-empirical models. Chen et al. developed an empirical band ratio algorithm to determine the optimal band ratio and its empirical function by using the model ranking method, which was applied to Landsat-8 images and obtained a good CDOM distribution and change situation, but the algorithm was limited to specific research sites [5]. Zhang et al. developed an algorithm for calculating the CDOM absorption coefficient from the remotely sensed reflectance R_{rs} (λ) using empirical and semi-empirical methods based on MODIS/Aqua satellite images and sample measured data [9]. Thayapurath et al. proposed a simple method to determine the slope of changes in the combined absorption spectra of CDOM and detritus, which improved the accuracy of CDOM inversion [10]. However, these empirical models overlook the influence of non-algal particles, resulting in uncertainties in experiments. Currently, research has shifted from empirical models to physical analytical models, offering a more systematic and rational approach. For instance, the physical analysis model, exemplified by the QAA algorithm, allows for the adjustment of algorithm parameters and reference wavelengths based on the characteristics of different lake waters. Additionally, the algorithm can differentiate between CDOM and NAP absorption coefficients, thereby reducing experimental uncertainties and facilitating its application to various complex water bodies. The QAA algorithm derived by Lee et al. was based on the radiative transfer equation, by which remotely sensed reflectance is inverted to perform absorption and scattering coefficients [11]. Yang et al., based on the bandwidth of the Moderate Resolution Imaging Spectrometer (MERIS), improved QAA to retrieve the inherent optical properties of cloudy inland waters. The results show that the improved performance of the QAA algorithm can be better applied to the MERIS satellite [12]. Martins et al. utilized simulated reflectance data from the Thematic Mapper (TM) sensor to assess empirical models and the QAA algorithm [13]. Ogashawara et al. successfully retrieved the spectral shapes of optically active constituents by fine-tuning the parameters of the QAA algorithm in CDOM-dominated waters while also maintaining the error margin within a reasonable range [14]. Pitarch and Vanhellemont proposed a semi-analytical algorithm called QAA-RGB, the total absorption coefficient, backscattering coefficient, and diffuse reflection attenuation coefficient derived from Landsat, Sentinel-2, and other satellite data exhibit a high degree of agreement with the measured data [15]. Santiago and Frey compared the empirical algorithm with several semi-analytical algorithms (including the QAA algorithm, GSM algorithm, and GSM-A) for CDOM in the Bering Sea, Chukchi Sea, and West Beaufort Sea within the Arctic region of the Pacific Ocean, and they found that the inversion accuracy of the QAA algorithm and GSM-A algorithm was higher [16]. Using 555nm as the reference band of the algorithm, Chen and Zhang established the inversion model QAA-RGR for the intrinsic light quantity of the East China Sea water body, and the algorithm can well retrieve the IOPs of the East China Sea [17]. Wang et al. proposed a QAA-CJ algorithm for turbid waters in the Yangtze River Estuary and East China Sea using 680 nm as a reference wavelength [18]. Zhu et al. developed an extended quasi-analytical algorithm (QAA-E) aimed at determining absorption coefficients for colored dissolved organic matter (CDOM) in the Mississippi and Atchafalaya River plume regions, as well as in the northern Gulf of Mexico [19]. Zhu and Yu improved the QAA-E algorithm and proposed a semi-analytic algorithm-quasi-analytic CDOM algorithm (QAA_CDOM algorithm) for inverting the CDOM absorption of (EO-1) Hyperion satellite images [20]. The water quality environment of Erhai Lake has gradually deteriorated. In some studies, it is feasible to analyze the composition and source of CDOM in lakes by fluorescence spectroscopy [21].

The QAA algorithm, proposed by Lee et al. in 2002, is a semi-analytical method based on the radiation transfer equation. It utilizes the relationship between remote sensing reflectance and the intrinsic optical properties of water bodies to retrieve the absorption coefficient of water-colored matter within the water body [11]. The algorithm consists

of three semi-analytic models, two analytic models, and two empirical models. The QAA_v6 algorithm is the fifth update of the QAA algorithm. Zhu et al. improved the decomposition mode of the QAA algorithm and proposed a semi-analytical algorithm, the Quasi-Analytical CDOM Algorithm (QAA_CDOM), which achieved better inversion results [20].

Hence, in this study, the physical analysis model QAA algorithm was employed, and it was applied to the Sentinel-3 OLCI satellite to achieve the inversion of CDOM concentration in Erhai Lake.

Therefore, the objectives of this study are as follows:

(1) Combining the QAA_v6 algorithm with QAA_CDOM, we propose a new algorithm, QAA_CDOM_680, which optimizes the reference wavelength based on in-situ hyperspectral data.

(2) The QAA_CDOM_680 algorithm was applied to Sentinel-3 OLCI satellite data to generate CDOM concentration maps for two field experiments conducted in Erhai Lake. This study aims to provide robust theoretical support and ensure accuracy for water quality monitoring and protection efforts in Erhai Lake.

II. STUDY AREA AND DATA

A. STUDY AREA

Erhai Lake, located in Dali Bai Autonomous Prefecture, Yunnan Province, is the second-largest freshwater lake in Yunnan Province and the seventh-largest freshwater lake in China (Figure 1). The lake area of Erhai is about 252 square kilometers, the water storage capacity reaches 2.95 billion cubic meters, the average water depth is 10 meters, the length of the lake is 42 kilometers from north to south, and the width of the lake is 3-9 kilometers from east to west, the lake starts from the south end of Eryuan County in the north and stops in the south of Xiaguan in Dali City [22]. There are 117 rivers of various sizes distributed around Erhai Lake, mainly including the Luo Shi River, Yongan River, Mi Tho River, Xi'er River, Cangshan Eighteen Streams, etc., of which only one natural outlet is located in the southwestern part [23]. The Erhai Lake is the source of drinking water for Dali, the center city of western Yunnan, and the core of the Cangshan Erhai National Nature Reserve and Scenic Spot, with various functions such as regulating the climate, providing water security for industrial and agricultural life, and maintaining biodiversity [24].

Erhai Lake, with its unique geographical advantages, has a low nutrient content and excellent water quality [25]. In recent decades, the increase in organic matter in the water due to the large influx of anthropogenic and agricultural pollutants into the lakes has led to increased humification of the lakes [26]. Phytoplankton grows in lakes, absorbing large amounts of nutrients and forming new organic matter as it degrades, exacerbating the eutrophication of lakes [27].

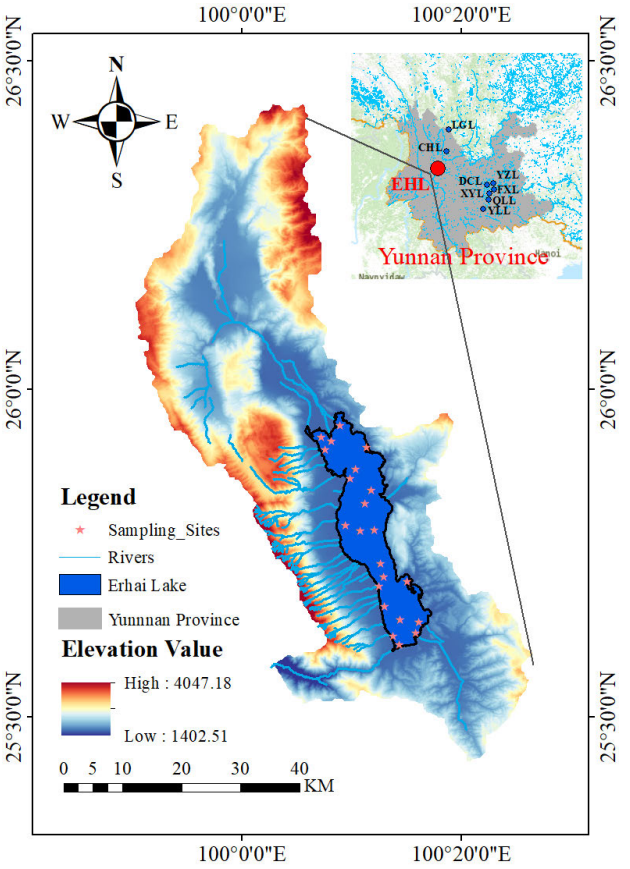

FIGURE 1. Map of the study area and sampling sites.

TABLE 1. In situ water column measurement times, data and satellite transit times.

Sampling Data	Number of Samples	The average of $a_{CDOM}(443)$(m^{-1})	The average of DOC(mg/L)	Image Data
March.05,2023	22	1.2573	26.7865	March.08,2023
June.05,2023	22	1.2492	25.3156	June.05,2023

B. IN SITU MEASUREMENT

The ground-test data utilized in this study were gathered during a field trip to Erhai Lake. Field sampling at Erhai Lake was conducted on March 5 and June 5, 2023, under selected clear-sky conditions. Point-by-point sampling was conducted sequentially at 22 stations, with samples selected from water bodies with a water surface of approximately 0–0.5m. The samples were collected from the water body of Erhai Lake. All samples were collected, preserved in brown glass vials, and stored at 4 degrees Celsius for further laboratory determination of CDOM absorption coefficients and other water column component concentrations. The results are shown in Table 1.

At each observation point, the AvaField spectrometer was used for in-situ measurements of the water body.

TABLE 2. Sentinel-3 band parameters.

Bands	Central Wavelength(nm)	Bandwidth(nm)	Spatial Resolution(m)
Band1	400	15	300
Band2	412.5	10	300
Band3	442.5	10	300
Band4	490	10	300
Band5	510	10	300
Band6	560	10	300
Band7	620	10	300
Band8	665	10	300
Band9	673.75	7.5	300
Band10	681.25	7.5	300
Band11	708.75	10	300
Band12	753.75	7.5	300
Band13	761.25	2.5	300
Band14	764.375	3.75	300
Band15	767.5	2.5	300
Band16	778.75	15	300
Band17	865	20	300
Band18	885	10	300
Band19	900	10	300
Band20	940	20	300
Band21	1029	40	300

The integration time for each observation was set to 0.02 seconds, and the spectral range measured for each curve was from 350 nm to 2500 nm, with a spectral resolution of 1 nm. A total of 22 representative measurement points were selected for field observations, and multiple measurements of the light from the water surface, whiteboard, and sky were taken at each point. To ensure the accuracy of spectral measurements, synchronous water sampling was conducted at each measurement point. The measurements were carried out between 10 a.m. and 2 p.m. under calm, clear skies.

C. SATELLITE DATA

The main role of the Sentinel-3 series of satellites, as a vital component of the ESA Copernicus program, is ocean forecasting and monitoring of the environment and climate. The binary stars were launched on February 16, 2016 and April 25, 2018, respectively. The star carries two sensors, OLCI and SLSTR. The OLCI sensor improves and innovates on the former AquaSat MERIS sensor by adding six new bands of information, for a total of 21 bands ranging from the visible to the near infrared (400 nm–1020 nm). It has the advantages of wide and narrow bandwidth, while the operation of the binary star system improves the temporal resolution of the images. The Sentinel-3 sensor is the Ocean and Land Color Instrument (OLCI) used in ENVISAT's MERIS to provide data continuity. The OLCI imaging spectrometer is a heap-scanning instrument with a spatial resolution of 300 m, measuring the Earth's reflected solar radiation in 21 spectral bands.

Since the algorithm requires an accuracy of 1nm for the entered wavelength number and the accuracy of the center wavelength of certain bands of Sentinel-3 OLCI does not meet this requirement, this study selects approximate values to align with the algorithm. Accordingly, bands 3, 4 and 10 of the satellite are chosen for calculation. Specifically, image dates of March 8 and June 5, 2023, were selected. The criteria for selecting these dates were low cloudiness and being within a week of field sampling. The wavelength bands selected for satellite data are shown in Table 2.

III. METHODS

A. IMAGE ATMOSPHERIC CORRECTION

To eliminate the effects of atmospheric water vapor, carbon dioxide, etc., on the reflection of features and the effects of scattering by atmospheric molecules and aerosols. This study uses the FLAASH atmospheric correction method in ENVI 5.6. FLAASH atmospheric corrections use the code of the MODTRAN4 radiative transfer model, which can handle any hyperspectral, satellite, and aeronautical data [28], [29]. The first step involves calculating the irradiance reflectance, denoted as R_t. The FLAASH atmospheric correction model equations are as follows [30]:

$$R_t = \frac{1-\rho_e S}{A}\left(L - B\frac{\rho_e}{1-\rho_e S} - L_a\right) \tag{1}$$

where L is the total radiant luminance received by the image element at the sensor; ρ_e is the average surface reflectance around the pixel; S is the atmospheric spherical albedo; L_a is the atmospheric backscattering radiance; A and B depend on two coefficients of atmospheric and geometric conditions.

R_{rs} is corrected by FLAASH atmospheric corrections calculated by removing reflectance from the water surface [31]:

$$R_{rs}(\lambda) = \frac{R_t}{\pi} - \frac{L_r(\theta, \varphi)}{E_d} \tag{2}$$

where L_r is the off-water irradiance, which carries information about the water column; E_d is the irradiance.

B. DATA PROCESSING

The radiation luminance of the water body, sky and reference plate is measured at each position using the method of water surface spectroscopy. Total water spectral radiation measured above the water surface [31], [32]:

$$L_{sw} = L_w + \gamma L_{sky} + L_g + L_{wc} \tag{3}$$

where L_{sw} represents the total signal measured by the instrument; L_w represents the outgoing reflected light scattered back into the instrument by the water column, which contains the upward portion of the scattered light from the water column and the reflected light from the bottom of the water; γL_{sky} represents the signal of the sky light entering the observing instrument after reflection at the water surface; γ is the reflectance of the sky light at the air-water interface; L_g denotes a solar flare produced by the random reflection of direct solar light by waves on the water surface; L_{wc} denotes information on sea surface whitecaps. The effects of surface whitecap information on the water column spectrum and the observation by surveyors. The OLCI image spectral profile was simulated using measured water reflectance data combined with the relative spectral response (RSR) function of Sentinel-3 satellites band1–band7 [33].

$$R_{rs}(B_i) = \frac{\int_{\lambda_m}^{\lambda_n} RSR(\lambda) * R_{rs}\_measured(\lambda)\, d\lambda}{\int_{\lambda_m}^{\lambda_n} RSR(\lambda)\, d\lambda} \tag{4}$$

where $R_{rs}\_measured(\lambda)$ is the in situ hyperspectral data and $R_{rs}(Bi)$ is the simulated remotely sensed reflectance in the i'th band of Sentinel-3, which is calculated by integrating $R_{rs}\_measured$ from λ_m to λ_n band ranges according to $RSR(\lambda)$.

In this study, the raw water samples were filtered through a 0.45 um MCE filtration membrane as well as a 0.22 um Millipore membrane, after which the filtrate was poured into a 10mm cuvette, and the absorbance from 200 nm to 800 nm was measured using a Shimadzu UV-2600 Spectrophotometer with Milli-Q as a reference [34]. The absorption coefficient $a_{CDOM}(\lambda)$ of CDOM is calculated as follows:

$$a_{CDOM}(\lambda) = 2.303 D(\lambda) / l \tag{5}$$

where λ is the wavelength (nm) and $a_{CDOM}(\lambda)$ is the absorption coefficient of CDOM (m^{-1}); $D(\lambda)$ is the absorbance; l is the light path (m) [35]. The absorption coefficients at wavelengths of 400 nm or 440 nm are usually used to express the concentration of CDOM [36]. It has been shown that the inversion effect of 443 nm applied to MERIS satellite is better [37]. Since the OLCI sensor, which is used to provide data continuity for MERIS, was chosen for this study, the CDOM absorption coefficient at 443 nm was selected.

C. QAA_CDOM_680 ALGORITHM

The QAA algorithm extends the reference wavelength to $\lambda_0 = 670$ nm to target inland lakes with complex optical properties [11]. Le et al. extended the reference wavelength λ_0 to 710 nm for the high-absorbing water body Taihu Lake and obtained better inversion results [38]. Extending the reference band to the near-infrared not only facilitates atmospheric corrections but also avoids the errors associated with the complexity of remotely sensed reflectance at short wavelengths. The QAA_CDOM algorithm changes the dataset for modeling to accommodate complex inland and nearshore water bodies. According to Lee's study, water bodies with a total absorption coefficient a (443) greater than 0.3 m^{-1} are considered highly absorbing [11]. The total absorption coefficient of Erhai Lake is smaller than that of Taihu Lake, and the reference wavelength should be less than 710 nm. Taking into account the concurrent availability of both in-situ hyperspectral data and Sentinel-3 OLCI band data, we have adjusted the reference wavelength for the inversion of CDOM concentration in Erhai Lake to the infrared band, specifically selecting Sentinel-3 OLCI band 10. According to Lee et al.'s study, to mitigate the effects of atmospheric correction errors in satellite-borne remote sensing images and the complexity of inherent optical characteristics at short wavelengths on the remote sensing reflectance at the reference wavelength, it is crucial to ensure that the remote sensing reflectance at the reference wavelength falls within a certain critical range [39].

The calculation formula is provided as follows:

$$R_{rs}(667) = 20\,(R_{rs}(\lambda_0))^{1.5} \tag{6}$$

$$R_{rs}(667) = 0.9\,(R_{rs}(\lambda_0))^{1.7} \tag{7}$$

The R_{rs} (667) of the Erhai water body is 0.0049 sr^{-1}. According to Eqs. 6 and 7, the R_{rs} (667) of Erhai falls within the critical range of remote sensing reflectance at the three reference wavelengths. However, it's noted that the critical range of 680 nm as the reference wavelength is smaller compared to 681 nm and 682 nm. Therefore, 680 nm is selected as the reference wavelength for the new algorithm.

The symbols related to the QAA algorithm are shown as indicated in Table 3.

Basic steps of the QAA_CDOM_680 algorithm:

Step 1: Calculation of remote sensing reflectance below the water surface $r_{rs}(\lambda)$:

$$r_{rs} = \frac{R_{rs}(\lambda)}{0.52 + 1.7 R_{rs}(\lambda)} \tag{8}$$

TABLE 3. List of notations.

Symbol	Description
$a(\lambda)$	Total absorption coefficient of water body
$a_w(\lambda)$	The absorption coefficient of pure water
$a_{dg}(\lambda)$	Absorption coefficient of non-algal particles and CDOM
$a_d(\lambda)$	Absorption coefficient of non-algae particles
$a_g(\lambda)$	Absorption coefficient of CDOM
$a_{ph}(\lambda)$	Absorption coefficient of phytoplankton
$b(\lambda)$	Scattering coefficient of water
$b_b(\lambda)$	Backscatter coefficient of water
$b_{bp}(\lambda)$	Backscatter coefficient of particles
$b_{bw}(\lambda)$	Backscattering coefficient of pure water
$R_{rs}(\lambda)$	Above-surface remote sensing reflectance
$r_{rs}(\lambda)$	Below-surface remote sensing reflectance

Step 2: When $k_0 = 6.807$ and $k_1 = 1.186$, u (λ) is calculated, and u (λ) is defined as the following equation:

$$u(\lambda) = 1 - \exp\left(\frac{-k_0 r_{rs}(\lambda)^{k_1}}{0.31 - r_{rs}(\lambda)}\right) \tag{9}$$

Step 3: The $R_{rs}(670)$ of Erhai Lake is greater than 0.0015, calculate a (λ_0):

$$a(\lambda_0) = a_w(680) + 0.39\left(\frac{R_{rs}(680)}{R_{rs}(443) + R_{rs}(490)}\right)^{1.14} \tag{10}$$

Step 4: Calculate $b_{bp}(\lambda)$ at reference wavelengths:

$$b_{bp}(\lambda_0) = \frac{u(\lambda_0) * a(\lambda_0)}{1 - u(\lambda_0)} - b_{bw}(680) \tag{11}$$

Step 5: Calculate $b_{bp}(443)$:

$$b_{bp}(443) = b_{bp}(\lambda_0)\left(\frac{\lambda_0}{443}\right)^{\eta} \tag{12}$$

$$\eta = y_0\left(1 - y_1 \exp\left(y_2 \frac{r_{rs}(443)}{r_{rs}(680)}\right)\right) \tag{13}$$

where coefficients y_0 =2.2, y_1 =1.2, y_2 =-0.9

Step 6: Calculate the total absorption coefficient a (443) at a wavelength of 443 nm:

$$a(443) = (1 - u(\lambda))\left(b_{bw}(\lambda) + b_{bp}(\lambda)\right)/u(\lambda) \tag{14}$$

Step 7: Calculate $a_p(443)$:

$$a_p(443) = j_1 b_{bp}(\lambda_0)^{j_2} \tag{15}$$

where coefficients $j_1 = 0.63$ and $j_2 = 0.88$;

Step 8: Calculate $a_{CDOM}(443)$:

$$a_{CDOM}(443) = a(443) - a_w(443) - a_p(443) \tag{16}$$

where the pure water absorption coefficient and backscattering coefficient are the same as in the QAA_v6 algorithm.

D. ALGORITHM SENSITIVITY ANALYSIS AND VALIDATION

According to existing research, optimizing the reference wavelength is a crucial step in algorithm adjustment. To further ascertain the performance enhancement brought by using 680nm as a reference wavelength in the new algorithm, the sensitivity of the remote sensing reflectance (R_{rs}) was analyzed. By introducing relative errors of -10%, -5%, 0%, 5%, and 10% in R_{rs}, the absorption coefficients were calculated for different error ranges.

This study uses an empirical approach to analyze and evaluate the results of CDOM inversion. First, the remotely sensed reflectance R_{rs} is calculated by the QAA_v6 algorithm to obtain the absorption coefficient of CDOM at wavelength 443 nm, $a_{CDOM}(443)$, and the algorithmic accuracy is verified for the calculated $a_{CDOM}(443)$ and the original for the measured $a_{CDOM}(443)$; secondly, the accuracy of the measured and predicted values is assessed through the coefficient of determination (R^2), root mean square error (RMSE), and mean absolute error (MAE).

The root mean square error (RMSE) is the arithmetic square root of the ratio of the sum of the squares of the differences between the predicted and true values for each group to the number of groups, n. The RMSE is a measure of the difference between the predicted and true values for each group compared to the number of groups, n. The RMSE is a measure of the difference between the predicted and true values for each group. The smaller the RMSE value, the higher the accuracy of the algorithm and the closer the predicted value is to the true value.

$$\mathrm{RMSE} = \sqrt{\frac{1}{n}\sum_{i=1}^{n}\left(Y_i^{estimated} - Y_i^{measured}\right)^2} \tag{17}$$

where RMSE represents the root mean square error, n represents the number of measurement groups, and $Yi^{estimated}$ and $Yi^{measured}$ represent the predicted and true values.

The mean absolute error (MAE) is used to represent the average of the absolute error between the true value and the predicted value. The smaller the MAE value, the closer the predicted value is to the true value.

$$\mathrm{MAE} = \frac{1}{n}\sum_{i=1}^{n}\left|Y_i^{estimated} - Y_i^{measured}\right| \tag{18}$$

where MAE denotes mean absolute error, n denotes the number of measurement groups, and $Yi^{estimated}$ and $Yi^{measured}$ denote predicted and true values.

IV. RESULTS

A. SPECTRAL ANALYSIS

Figure 2 illustrates the reflectance spectrum of the water column in Erhai Lake in June. The reflectance curve of the Erhai water body exhibits a general trend of increasing and then decreasing, interspersed with several peaks and troughs. In the wavelength range of 400nm to 570nm, the reflectance increases with wavelength, while it gradually decreases in the range from 570 nm to 800 nm, with peaks and troughs observed intermittently within this range.

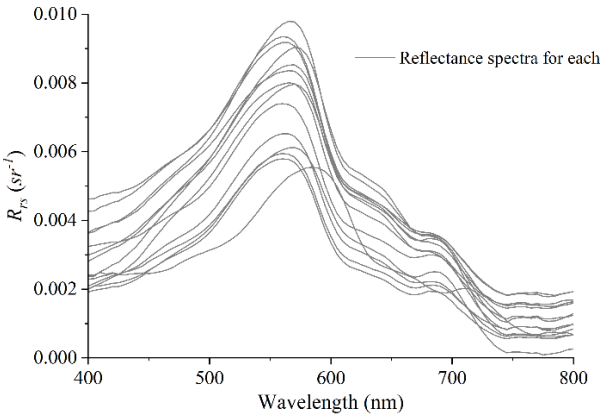

FIGURE 2. Measured reflectance spectra of the erhai lake surface.

Spectral curves reflect the optical properties of the water body, and these spectra are typical of freshwater spectral features. Remote sensing reflectivity of water bodies is lower in the blue band, influenced by the higher absorption capacity of algae and CDOM; the spectrum has peaks near 570 nm and 700 nm. At 570 nm in the blue-green band, due to the small absorption coefficient of phytoplankton and the effect of backscattering by non-algal particles, it shows a peaked condition. In the red-light band, the absorption of chlorophyll leads to an absorption peak at 670 nm. The peak at 700 nm is caused by a combination of phytoplankton pigments and absorption by the water column itself.

The measured water reflectance data is combined with the spectral response functions of the Sentinel-3 OLCI satellite bands to simulate the spectral profile of the OLCI imagery. The results show that the values of the simulated reflectance have a tendency to agree with the in situ spectral measurements, preserving the characteristic properties of the original reflectance spectra. There are distinct reflective features around 570 nm and 700 nm, with a gradual increase in reflectance from 400 nm to 570 nm and a gradual decrease from 570 nm to 800 nm, with peaks and valleys in the range and the highest and lowest reflectance values in the green and near-infrared wavelength bands. The results for the 400-900nm wavelength band are shown in Figure 3.

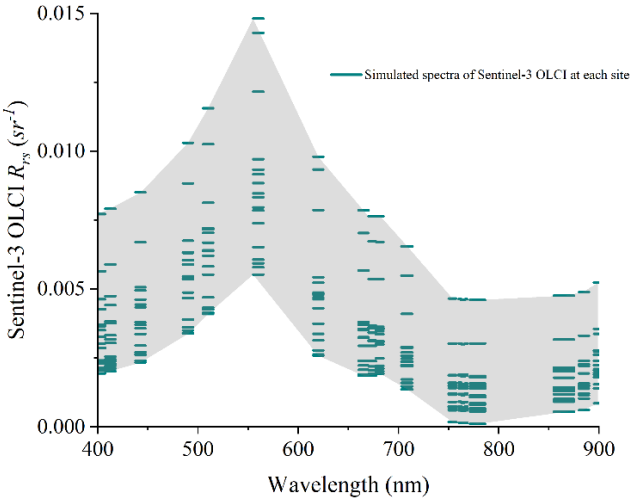

FIGURE 3. Sentinel-3 simulated band reflectance.

The CDOM absorption spectra for Erhai Lake in June were calculated using equation (6) mentioned above (Figure 4). The absorption characteristics of all the sample points are very similar; the difference between the values is small, with good consistency: the absorption is stronger at short wavelengths, and the absorption coefficient gradually decreases with the increase in wavelengths, and the value tends to be close to zero at 700 nm.

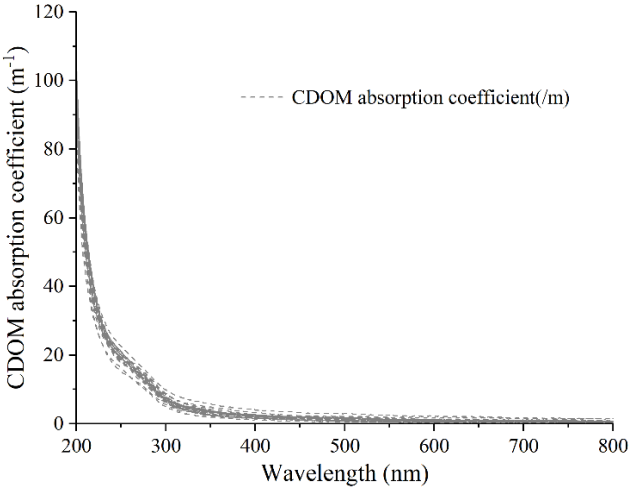

FIGURE 4. CDOM absorption spectrum of the erhai lake.

B. SENSITIVITY ANALYSIS AND VALIDATION

Three measured spectral curves of Erhai Lake were selected for sensitivity analysis, and the three spectral curves were the

TABLE 4. Inversion values of CDOM after introducing errors in different spectral curves.

Wavelength (nm)		Relative Rrs errors (%)				
		-10	-5	0	5	10
max	443 490 680	0.7906	0.7789	0.7670	0.7550	0.7429
average	443 490 680	0.8864	0.8826	0.8790	0.8754	0.8718
min	443 490 680	0.8212	0.8183	0.8155	0.8130	0.8105

highest reflectance value, the lowest reflectance value, and the average value. Table 4 shows the inversion values of the algorithm after introducing errors for reflectivity. After introducing different errors to the maximum reflectance value, the maximum difference of the inversion value is 0.0241(m^{-1}), the maximum difference of the minimum reflectance value is 0.0057(m^{-1}), and the average difference is 0.00074(m^{-1}). It can be seen that the new algorithm can still maintain good robustness in the error sweep.

Application of in situ hyperspectral data R_{rs} (λ) to invert was determined to be 11. The validation results of the QAA_v6 and QAA_CDOM algorithms are shown in Figure 5. The QAA_v6 algorithm R^2 is 0.44, the root mean square error (RMSE) is 0.615, and the mean absolute error (MAE) is 0.5653. The QAA_CDOM algorithm R^2, RMSE, and MAE are 0.51, 0.2235, and 0.1728, respectively. The QAA_CDOM algorithm has improved the accuracy of inverting the CDOM absorption coefficients of inland lakes compared to the QAA_v6 algorithm.

The QAA_CDOM algorithm was improved by the analysis in Chapter 3, and the reference wavelength of the QAA_CDOM algorithm was optimized to 680 nm. The QAA_CDOM_680 algorithm R^2 is 0.63, RMSE is 0.1935, and MAE is 0.1699. The root mean square error is improved by 0.03 compared to the QAA_CDOM algorithm, and the MAE is improved by 0.0029 compared to the QAA_CDOM algorithm. The new algorithm has a certain improvement in ergodic applicability, and the results are shown in Figure 6. The accuracy validation results of the a_{CDOM} (443) retrieval algorithms are shown in Table 5. Three algorithms, QAA_CDOM_680, adjust the corresponding reference wavelength on the basis of the QAA_CDOM algorithm, and the accuracy is improved; R^2 reaches 0.63, the root mean square error (RMSE) is minimized to 0.1935, and the mean absolute value error is 0.1699. The QAA_CDOM algorithm has an R^2 of 0.51, a root mean square error of 0.2235, and a mean absolute error of 0.1728. The QAA_v6 algorithm has an R^2 of 0.44, a root mean square error of 0.615, and a mean absolute error of 0.5653.

The error bars are shown in Figure 7, and the error bars are set according to the RMSE. Of the three algorithms, the QAA_v6 algorithm has the largest error, the QAA_CDOM

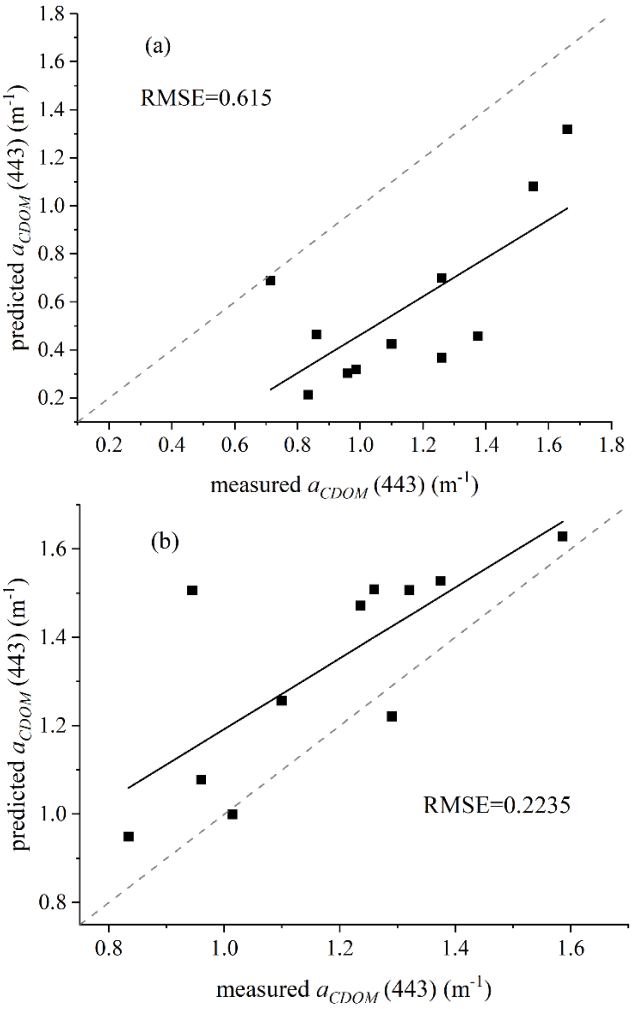

FIGURE 5. (a) QAA_v6 algorithm accuracy validation, (b) QAA_CDOM algorithm accuracy validation.

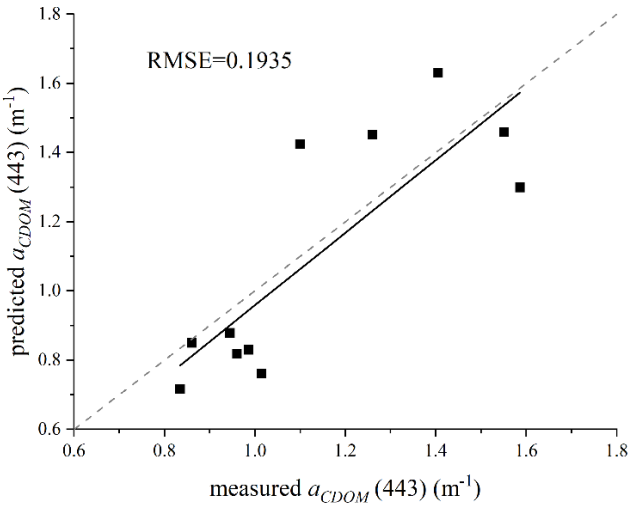

FIGURE 6. QAA_CDOM_680 algorithm accuracy validation.

algorithm has a large deviation from the measured value at individual points, and the QAA_CDOM_680 algorithm is relatively stable, with a minimum deviation at every point.

TABLE 5. Verification of the accuracy of the three algorithms.

algorithms	R^2	RMSE(m^{-1})	MAE(m^{-1})	n
QAA_v6	0.44	0.6150	0.5653	11
QAA_CDOM	0.51	0.2235	0.1728	11
QAA_CDOM_680	0.63	0.1935	0.1699	11

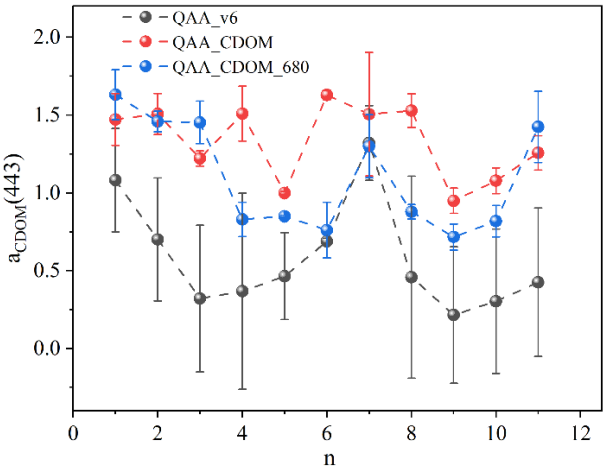

FIGURE 7. Error bar analysis of QAA_v6, QAA_CDOM, and QAA_CDOM_680 algorithms.

C. APPLIED IN ACTUAL SATELITE DATA

The QAA_CDOM_680 algorithm was applied to Sentinel-3 OLCI data for two scenes with less cloud coverage on March 8, 2023, and June 5, 2023. Due to the high-altitude nature of

Yunnan province, there is typically higher cloud coverage, making the availability of Sentinel-3 OLCI image data limited. Therefore, the image was chosen to be associated with field sampling over no more than three days. The inversion results of the algorithm are shown in Figure 8, clearly depicting the gradient distribution of CDOM content in Erhai Lake.

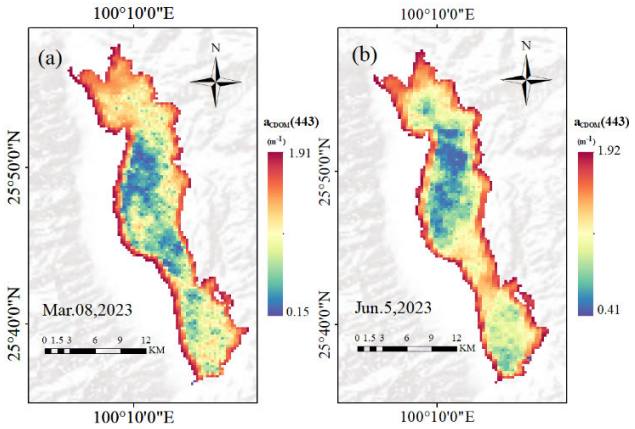

FIGURE 8. Inversion of CDOM absorption coefficients from Sentinel-3 OLCI images. (a) 8 March 2023, inversion results; (b) 5 June 2023, inversion results.

In terms of spatial distribution, the main feature of $a_{CDOM}(443)$ in Erhai Lake is higher concentrations along the entire lake shoreline, relatively lower concentrations in the lake center, higher concentrations in the northern region, and lower concentrations in the southern region. The maximum value observed across the entire lake reaches 1.92 (m^{-1}), while the minimum value is 0.15 (m^{-1}). It can be seen that the lake areas with higher CDOM concentrations are located near the shore and in the northern region. The higher concentration along the shoreline is mainly due to the surface runoff from the 18 streams of Cangshan Mountain flowing into Erhai Lake, which brings in a large amount of organic matter. The high concentration in the north is mainly due to the large number of wetland ecosystems in the north, where dead leaves and branches fall into the lake and the humus content in the water is high. The lower concentrations in the southern part of Erhai Lake are better controlled by humans.

Combining the above experimental results, the satellite inversion results were cross-validated using synchronized sampling data on March 5 and June 5, 2023, and the results were determined by the validation model determinations R^2, RMSE, and MAE. The $a_{CDOM}(443)$ satellite inversion validation results are shown in Table 6. The two-scene data R^2 were 0.42 and 0.48, RMSE were 0.2298 and 0.1968, and MAE were 0.1819 and 0.1617, respectively.

TABLE 6. Evaluation of the accuracy of CDOM concentration inversion based on the QAA_CDOM_680 algorithm Sentinel-3 OLCI.

Date	Calibration Model	R^2	RMSE(m^{-1})	MAE(m^{-1})	n
March.08,2023	y=0.2565x+0.8985	0.42	0.2298	0.1819	10
June.05,2023	y=0.8806x+0.2346	0.48	0.1968	0.1617	10

V. DISCUSSION

CDOM, as an important factor of beam attenuation in water bodies, is important to study its remote sensing inversion [40]. However, fewer studies have been conducted on CDOM relative to chlorophyll a (Chl-a) as well as total suspended matter (TSM). Most CDOM studies at this stage are based on empirical or semi-empirical algorithms (methods such as band ratios), but they are susceptible to the limitations of the watershed, and therefore there is a need to improve CDOM inversion methods that are applicable to a wide range of water body types [38], [41], [42]. The improved QAA_CDOM_680 algorithm in this study shows a significant enhancement in applicability compared to the QAA_v6 and QAA_CDOM algorithms in Erhai Lake. However, further research is needed to investigate the practical application of the QAA_CDOM_680 algorithm in the future.

Since no additional relevant datasets were collected in this study, accuracy verification was conducted using two field sampling measurements from Erhai Lake. Comparing the QAA_CDOM_680 algorithm proposed in this study

with the previous QAA_v6 and QAA_CDOM algorithms, it was observed that optimizing the reference wavelength can enhance the algorithm's applicability in Erhai Lake. In future research, we will incorporate different datasets for validation and comparison. The QAA_CDOM_680 algorithm is more suitable for the water body of Erhai Lake through the accuracy analysis. Changing the reference wavelength of the algorithm for different water bodies is a worthwhile research problem. Therefore, building upon the QAA algorithm, it is imperative to conduct reasonable optimization and adjustment of algorithm model parameters and reference wavelengths for research areas exhibiting diverse water characteristics. This may involve extending reference wavelengths based on specific water areas or different sensors, as well as fine-tuning algorithm parameters using extensive field datasets, all aimed at enhancing experimental accuracy.

The study of the QAA algorithm starts with the empirical and semi-analytical models in the algorithm, while the decomposition of $a(\lambda)$ is a worthwhile research direction [19]. Although the accuracy of the QAA_CDOM_680 inversion in Erhai Lake has improved, there are still some factors that lead to the uncertainty of the inversion. First, the QAA_v6 algorithm has step-by-step errors for $a(\lambda)$ and $b(\lambda)$, which accumulate and thus image the inversion accuracy of CDOM. Usually, in near-shore or inland water bodies, the QAA algorithm needs to optimize the model parameters according to different study areas, such as adjusting the reference wavelength, etc., in order to better invert the intrinsic optical quantity of the water body. The second is the separation algorithm for the total absorption coefficient. Further collection of a lot of water samples from different regions is needed to improve the accuracy of the algorithm and the calibration of the bio-optical model. The separation algorithm of QAA_CDOM was used and not improved in this experiment.

Currently, remote sensing technology has been widely used in water quality parameter inversion studies, but it is still difficult to reach the precision stage. Satellite inversion needs to take into account the effects of clouds and atmospheric corrections. Atmospheric correction is a key process in image-based CDOM estimation, and it largely determines a model's input data (R_{rs}). Modeling algorithms applied to remotely sensed imagery and atmospheric correction is an issue that needs to be addressed squarely. Only by continuously improving the atmospheric correction model can we obtain more accurate remote sensing reflectance on the water surface, reduce the experimental inversion error, and improve the experimental inversion accuracy. At the same time, the influence of clouds cannot be ignored, and it is of great significance to break through the limitation of clouds and combine MODIS, Landsat-8, or Sentinel-2 multi-source remote sensing data to make long-term observations for the study of organic matter concentration.

In this study, a novel algorithm, QAA_CDOM_680, based on in-situ hyperspectral data adjustment, was used to evaluate its accuracy and applicability in Erhai Lake through two field measurements. Satellite-ground synchronous inversion results indicate the algorithm's strong suitability for Erhai Lake. However, this research did not conduct qualitative and quantitative analyses of Erhai CDOM over an extended period using the new algorithm. Given the long-term fluctuating environmental conditions of Erhai Lake, the efficacy of the algorithm may be influenced by optimizing the reference wavelength across different datasets over time. Thus, continuous attention should be given to the algorithm's stability for long-term series monitoring. Adjustments to corresponding parameters may be necessary to uphold the algorithm's accuracy and reliability as temporal conditions evolve.

VI. CONCLUSION

In this study, we compared and analyzed the QAA_v6 algorithm and the QAA_CDOM algorithm based on spectral data measured in the field and combined with Sentinel-3 OLCI data. Building upon these two algorithms, we developed a new QAA_CDOM_680 inversion algorithm. Additionally, we thoroughly examined and discussed the applicability of this algorithm in the context of Erhai Lake. The main conclusions are as follows:

1) Comparing the three QAA algorithms, it is evident that the QAA_v6 algorithm ($R^2 = 0.44$, RMSE $= 0.615$) exhibits lower applicability in Erhai Lake. Conversely, when applied to modeling the nearshore water body dataset, the QAA_CDOM algorithm demonstrates higher accuracy ($R^2 = 0.51$) and improved applicability compared to other algorithms, with a lower root mean square error (RMSE $= 0.2235$). By adjusting the reference wavelengths based on the latter, the QAA_CDOM_680 algorithm achieves an R^2 of 0.61 and reduces the RMSE to 0.2136, significantly enhancing the accuracy of the algorithm in inverting the intrinsic optical quantities of the water body in Erhai Lake and potentially other inland lakes as well. Moreover, sensitivity analysis of the algorithm indicates a certain level of robustness.

2) The results of the inverse performances of the Sentinel-3 OLCI images of the two views: R^2 were 0.42 and 0.48, the root mean square errors (RMSE) were 0.2298 and 0.1968, and the mean absolute errors (MAE) were 0.1819 and 0.1617. The accuracy verification results demonstrate the stability of the Sentinel-3 inversion outcomes for Erhai Lake. In terms of the spatial distribution, the Erhai lake shore is high and the lake center is low, and the north is high and the south is low. The results of this study provide algorithmic support for the remote sensing monitoring and analysis of the Erhai CDOM.

DECLARATION OF COMPETING INTEREST

The authors declare that they have no known competing financial interests or personal relationships that could have appeared to influence the work reported in this paper.

DATA AVAILABILITY

The measured data utilized in the algorithms presented in this paper is currently not publicly available; however, they can be made available to interested parties upon request from the authors.

REFERENCES

[1] P. L. Brezonik, L. G. Olmanson, J. C. Finlay, and M. E. Bauer, "Factors affecting the measurement of CDOM by remote sensing of optically complex inland waters," *Remote Sens. Environ.*, vol. 157, pp. 199–215, Feb. 2015, doi: 10.1016/j.rse.2014.04.033.

[2] P. G. Coble, "Marine optical biogeochemistry: The chemistry of ocean color," *Chem. Rev.*, vol. 107, no. 2, pp. 402–418, Feb. 2007.

[3] J. T. O. Kirk, "Light and photosynthesis in aquatic ecosystems," *ACTA Physiol. Plant.*, vol. 17, p. 100, Apr. 1995.

[4] N. B. Nelson, D. A. Siegel, and A. F. Michaels, "Seasonal dynamics of colored dissolved material in the Sargasso sea," *Deep Sea Res. Part I, Oceanographic Res. Papers*, vol. 45, no. 6, pp. 931–957, Jan. 1998.

[5] J. Chen, W.-N. Zhu, Y. Q. Tian, and Q. Yu, "Estimation of colored dissolved organic matter from Landsat-8 imagery for complex inland water: Case study of Lake Huron," *IEEE Trans. Geosci. Remote Sens.*, vol. 55, no. 4, pp. 2201–2212, Apr. 2017, doi: 10.1109/TGRS.2016.2638828.

[6] C. A. Stedmon, S. Markager, and H. Kaas, "Optical properties and signatures of chromophoric dissolved organic matter (CDOM) in Danish coastal waters," *Estuarine, Coastal Shelf Sci.*, vol. 51, no. 2, pp. 267–278, Aug. 2000, doi: 10.1006/ecss.2000.0645.

[7] E. Organelli, A. Bricaud, B. Gentili, D. Antoine, and V. Vellucci, "Retrieval of colored detrital matter (CDM) light absorption coefficients in the Mediterranean Sea using field and satellite ocean color radiometry: Evaluation of bio-optical inversion models," *Remote Sens. Environ.*, vol. 186, pp. 297–310, Dec. 2016, doi: 10.1016/j.rse.2016.08.028.

[8] C. E. Del Castillo and R. L. Miller, "On the use of ocean color remote sensing to measure the transport of dissolved organic carbon by the Mississippi river plume," *Remote Sens. Environ.*, vol. 112, no. 3, pp. 836–844, Mar. 2008, doi: 10.1016/j.rse.2007.06.015.

[9] H. Zhang, B. Yao, S. Wang, and G. Wang, "Remote sensing estimation of the concentration and sources of coloured dissolved organic matter based on MODIS: A case study of erhai lake," *Ecol. Indicators*, vol. 131, Nov. 2021, Art. no. 108180, doi: 10.1016/j.ecolind.2021.108180.

[10] S. Thayapurath, A. B. Dias, E. J. A. Desa, and A. Sahay, "An algorithm to determine the slope of the spectral absorption of colored dissolved organic matter (CDOM) and detritus," *J. Indian Soc. Remote Sens.*, vol. 46, no. 4, pp. 625–631, Apr. 2018, doi: 10.1007/s12524-017-0722-6.

[11] Z. Lee, K. L. Carder, and R. A. Arnone, "Deriving inherent optical properties from water color: A multiband quasi-analytical algorithm for optically deep waters," *Appl. Opt.*, vol. 41, no. 27, p. 5755, Sep. 2002, doi: 10.1364/ao.41.005755.

[12] W. Yang, B. Matsushita, J. Chen, K. Yoshimura, and T. Fukushima, "Retrieval of inherent optical properties for turbid inland waters from remote-sensing reflectance," *IEEE Trans. Geosci. Remote Sens.*, vol. 51, no. 6, pp. 3761–3773, Jun. 2013, doi: 10.1109/TGRS.2012.2220147.

[13] S. Martins, K. Chokmani, E. Alcântara, I. Ogashawara, and A. El-Alem, "Mapping the coloured dissolved organic matter absorption coefficient in a eutrophic reservoir using remotely sensed images," *Inland Waters*, vol. 8, no. 4, pp. 488–504, Oct. 2018, doi: 10.1080/20442041.2018.1482153.

[14] I. Ogashawara, D. R. Mishra, R. F. F. Nascimento, E. H. Alcântara, M. Kampel, and J. L. Stech, "Re-parameterization of a quasi-analytical algorithm for colored dissolved organic matter dominant inland waters," *Int. J. Appl. Earth Observ. Geoinf.*, vol. 53, pp. 128–145, Dec. 2016, doi: 10.1016/j.jag.2016.09.001.

[15] J. Pitarch and Q. Vanhellemont, "The QAA-RGB: A universal three-band absorption and backscattering retrieval algorithm for high resolution satellite sensors. Development and implementation in ACOLITE," *Remote Sens. Environ.*, vol. 265, Nov. 2021, Art. no. 112667, doi: 10.1016/j.rse.2021.112667.

[16] M. I. Santiago and K. E. Frey, "Assessment of empirical and semi-analytical algorithms using MODIS-Aqua for representing in-situ chromophoric dissolved organic matter (CDOM) in the bering, chukchi, and Western Beaufort seas of the Pacific Arctic region," *Remote Sens.*, vol. 13, no. 18, p. 3673, Sep. 2021, doi: 10.3390/rs13183673.

[17] S. Chen and T. Zhang, "Evaluation of a QAA-based algorithm using MODIS land bands data for retrieval of IOPs in the eastern China seas," *Opt. Exp.*, vol. 23, no. 11, p. 13953, Jun. 2015, doi: 10.1364/oe.23.013953.

[18] Y. Wang, F. Shen, L. Sokoletsky, and X. Sun, "Validation and calibration of QAA algorithm for CDOM absorption retrieval in the Changjiang (Yangtze) estuarine and coastal waters," *Remote Sens.*, vol. 9, no. 11, p. 1192, Nov. 2017, doi: 10.3390/rs9111192.

[19] W. Zhu, Q. Yu, Y. Q. Tian, R. F. Chen, and G. B. Gardner, "Estimation of chromophoric dissolved organic matter in the Mississippi and atchafalaya river plume regions using above-surface hyperspectral remote sensing," *J. Geophys. Res.*, vol. 116, no. C2, pp. 1–22, Feb. 2011, doi: 10.1029/2010jc006523.

[20] W. Zhu and Q. Yu, "Inversion of chromophoric dissolved organic matter from EO-1 hyperion imagery for turbid estuarine and coastal waters," *IEEE Trans. Geosci. Remote Sens.*, vol. 51, no. 6, pp. 3286–3298, Jun. 2013, doi: 10.1109/TGRS.2012.2224117.

[21] L. Zhang, K. Xu, S. Wang, S. Wang, Y. Li, Q. Li, and Z. Meng, "Characteristics of dissolved organic nitrogen in overlying water of typical lakes of Yunnan Plateau, China," *Ecol. Indicators*, vol. 84, pp. 727–737, Jan. 2018, doi: 10.1016/j.ecolind.2017.09.038.

[22] J. Li, Y. Bai, and J. M. Alatalo, "Impacts of rural tourism-driven land use change on ecosystems services provision in erhai lake basin, China," *Ecosystem Services*, vol. 42, Apr. 2020, Art. no. 101081, doi: 10.1016/j.ecoser.2020.101081.

[23] G. Liu, Z. Liu, B. Gu, J. M. Smoak, and Z. Zhang, "How important are trophic state, macrophyte and fish population effects on cladoceran community? A study in lake erhai," *Hydrobiologia*, vol. 736, no. 1, pp. 189–204, Sep. 2014, doi: 10.1007/s10750-014-1906-5.

[24] C. Xiaohua, Q. Xiaoyong, L. Xiaoping, W. Zhihong, and H. Shuangqing, "Long-term trend of eutrophication state of lake erhai in 1988-2013 and analyses of its socio-economic drivers," *J. Lake Sci.*, vol. 30, no. 1, pp. 70–78, 2018, doi: 10.18307/2018.0107.

[25] N. Ji, S. Wang, and L. Zhang, "Characteristics of dissolved organic phosphorus inputs to freshwater lakes: A case study of lake erhai, Southwest China," *Sci. Total Environ.*, vols. 601–602, pp. 1544–1555, Dec. 2017, doi: 10.1016/j.scitotenv.2017.05.265.

[26] H. C. Guo, L. Liu, G. H. Huang, G. A. Fuller, R. Zou, and Y. Y. Yin, "A system dynamics approach for regional environmental planning and management: A study for the Lake Erhai basin," *J. Environ. Manage.*, vol. 61, no. 1, pp. 93–111, Jan. 2001, doi: 10.1006/jema.2000.0400.

[27] D. A. Aurin and H. M. Dierssen, "Advantages and limitations of ocean color remote sensing in CDOM-dominated, mineral-rich coastal and estuarine waters," *Remote Sens. Environ.*, vol. 125, pp. 181–197, Oct. 2012, doi: 10.1016/j.rse.2012.07.001.

[28] S. M. Adler-Golden, P. K. Acharya, A. Berk, M. W. Matthew, and D. Gorodetzky, "Remote bathymetry of the littoral zone from AVIRIS, LASH, and QuickBird imagery," *IEEE Trans. Geosci. Remote Sens.*, vol. 43, no. 2, pp. 337–347, Feb. 2005, doi: 10.1109/TGRS.2004.841246.

[29] W. J. Moses, A. A. Gitelson, R. L. Perk, D. Gurlin, D. C. Rundquist, B. C. Leavitt, T. M. Barrow, and P. Brakhage, "Estimation of chlorophyll—A concentration in turbid productive waters using airborne hyperspectral data," *Water Res.*, vol. 46, no. 4, pp. 993–1004, Mar. 2012, doi: 10.1016/j.watres.2011.11.068.

[30] R. Zhang, Z. Zheng, G. Liu, C. Du, C. Du, S. Lei, Y. Xu, J. Xu, M. Mu, S. Bi, and J. Li, "Simulation and assessment of the capabilities of orbita hyperspectral (OHS) imagery for remotely monitoring chlorophyll—A in eutrophic Plateau lakes," *Remote Sens.*, vol. 13, no. 14, p. 2821, Jul. 2021, doi: 10.3390/rs13142821.

[31] C. D. Mobley, "Estimation of the remote-sensing reflectance from above-surface measurements," *Appl. Opt.*, vol. 38, no. 36, p. 7442, Dec. 1999, doi: 10.1364/ao.38.007442.

[32] J.-W. Tang, G.-L. Tian, X.-Y. Wang, X.-M. Wang, and Q.-J. Song, "The methods of water spectra measurement and analysis I, above-water method," *J. Remote Sens.*, vol. 8, pp. 37–44, Jan. 2004.

[33] S. Trigg and S. Flasse, "Characterizing the spectral-temporal response of burned Savannah using in situ spectroradiometry and infrared thermometry," *Int. J. Remote Sens.*, vol. 21, no. 16, pp. 3161–3168, Jan. 2000, doi: 10.1080/01431160050145045.

[34] P. Kowalczuk, J. Sto-Egiert, W. J. Cooper, R. F. Whitehead, and M. J. Durako, "Characterization of chromophoric dissolved organic matter (CDOM) in the Baltic sea by excitation emission matrix fluorescence spectroscopy," *Mar. Chem.*, vol. 96, nos. 3–4, pp. 273–292, Sep. 2005, doi: 10.1016/j.marchem.2005.03.002.

[35] C. G. Griffin, J. W. McClelland, K. E. Frey, G. Fiske, and R. M. Holmes, "Quantifying CDOM and DOC in major Arctic rivers during ice-free conditions using Landsat TM and ETM+ data," *Remote Sens. Environ.*, vol. 209, pp. 395–409, May 2018, doi: 10.1016/j.rse.2018.02.060.
[36] J. Xu, C. Fang, D. Gao, H. Zhang, C. Gao, Z. Xu, and Y. Wang, "Optical models for remote sensing of chromophoric dissolved organic matter (CDOM) absorption in Poyang lake," *ISPRS J. Photogramm. Remote Sens.*, vol. 142, pp. 124–136, Aug. 2018, doi: 10.1016/j.isprsjprs.2018.06.004.
[37] T. Kutser, C. Verpoorter, B. Paavel, and L. J. Tranvik, "Estimating lake carbon fractions from remote sensing data," *Remote Sens. Environ.*, vol. 157, pp. 138–146, Feb. 2015, doi: 10.1016/j.rse.2014.05.020.
[38] C. Feng Le, Y. Mei Li, Y. Zha, D. Sun, and B. Yin, "Validation of a quasi-analytical algorithm for highly turbid eutrophic water of Meiliang bay in Taihu Lake, China," *IEEE Trans. Geosci. Remote Sens.*, vol. 47, no. 8, pp. 2492–2500, Aug. 2009, doi: 10.1109/TGRS.2009.2015658.
[39] Z. Lee, B. Lubac, J. Werdell, and R. Arnone, "An update of the quasi-analytical algorithm (QAA_v5)," *Int. Ocean Color Group Softw. Rep.*, vol. 1, pp. 1–9, Feb. 2009.
[40] F. Cao, M. Tzortziou, C. Hu, A. Mannino, C. G. Fichot, R. Del Vecchio, R. G. Najjar, and M. Novak, "Remote sensing retrievals of colored dissolved organic matter and dissolved organic carbon dynamics in North American estuaries and their margins," *Remote Sens. Environ.*, vol. 205, pp. 151–165, Feb. 2018, doi: 10.1016/j.rse.2017.11.014.
[41] S. Maritorena, D. A. Siegel, and A. R. Peterson, "Optimization of a semianalytical ocean color model for global-scale applications," *Appl. Opt.*, vol. 41, no. 15, p. 2705, May 2002, doi: 10.1364/ao.41.002705.
[42] A. Morel and B. Gentili, "A simple band ratio technique to quantify the colored dissolved and detrital organic material from ocean color remotely sensed data," *Remote Sens. Environ.*, vol. 113, no. 5, pp. 998–1011, May 2009, doi: 10.1016/j.rse.2009.01.008.

ZHENGNAN ZENG was born in April 1999. He received the Bachelor of Science degree in geographic information science, in 2021. He is currently pursuing the master's degree in surveying and mapping engineering with the School of Land and Resource Engineering, Kunming University of Science and Technology. His research interest includes remote sensing of lake water environment.

BO-HUI TANG (Senior Member, IEEE) received the B.S. degree in cartography and geographical information system from Wuhan University, Wuhan, China, in 1999, the M.S. degree in cartography and geographical information system from China Remote Sensing Satellite Ground Station, Chinese Academy of Sciences, Beijing, China, in 2004, and the Ph.D. degree in cartography and geographical information system from the Institute of Geographic Sciences and Natural Resources Research, Chinese Academy of Sciences, Beijing, in 2007.

He is currently a Research Fellow with Kunming University of Science and Technology and the Institute of Geographic Sciences and Natural Resources Research, Chinese Academy of Sciences. His main research interests include the retrieval and validation of land surface net radiation and land surface temperature and emissivity.

DONG WANG (Student Member, IEEE) was born in December 1997. He received the B.Eng. degree in surveying and mapping engineering, in June 2020. He is currently pursuing the Ph.D. degree in mapping science and technology with the Faculty of Land and Resources Engineering, Kunming University of Science and Technology. His research interest includes remote sensing of lake water environment.

LIANG HUANG received the B.S. degree in surveying and mapping engineering from Hunan City University, Hunan, China, in 2009, and the M.S. degree in cartography and geographic information engineering and the Ph.D. degree in earth exploration and information technology from Kunming University of Science and Technology, Kunming, China, in 2011 and 2015, respectively.

His research interests include the high spatial resolution remote sensing image segmentation and fine extraction and recognition of plateau crops. He is currently a member of the Plateau Remote Sensing Innovation Research Team, Kunming University of Science and Technology.

GUOKUN CHEN received the B.S. degree in cartography and geographical information system from Hefei University of Technology, Hefei, China, in 2011, the M.S. degree in geography and remote sensing science from Beijing Normal University, Beijing, China, in 2014, and the Ph.D. degree from the Institute of Remote Sensing and Digital Earth, Chinese Academy of Sciences, in 2019.

His research interests include the comprehensive evaluation of plateau lakes and regional ecological environment. He is currently a member of the Plateau Remote Sensing Innovation Research Team, Kunming University of Science and Technology.

ZHONGXI GE received the B.S. degree in land resource management from Huazhong Agriculture University, Hubei, China, in 2012, the M.S. degree in land resource management from Yunnan University, Kunming, China, in 2015, and the Ph.D. degree in physical geography from Southwest University, in 2022.

His research interests include the remote sensing application in ecology and carbon cycle. He is currently a member of the Plateau Remote Sensing Innovation Research Team, Kunming University of Science and Technology.